THE JOURNAL OF PHYSICAL CHEMISTRY C

Article

pubs.acs.org/JPCC

Facile Synthesis of MnO_2/CNTs Composite for Supercapacitor Electrodes with Long Cycle Stability

Li Li,[†,‡] Zhong A. Hu,[*,†] Ning An,[†] Yu Y. Yang,[†] Zhi M. Li,[†] and Hong Y. Wu[†]

[†]Key Laboratory of Eco-Environment-Related Polymer Materials of Ministry of Education, Key Laboratory of Polymer Materials of Gansu Province, College of Chemistry and Chemical Engineering, Northwest Normal University, Lanzhou, Gansu 730070, China

[‡]College of Chemical Engineering, Northwest University for Nationalities, Lanzhou, Gansu 730030, China

Supporting Information

ABSTRACT: The MnO_2/carbon nanotubes (CNTs) composites were prepared through a modified one-pot reaction process, in which CNTs were coated by cross-linked MnO_2 flakes uniformly. The composition, morphology, and microstructure of the products were characterized using TG, XRD, XPS, Raman, FESEM, TEM, and STEM. It reveals that the MnO_2 layer stands on the sidewalls of the inner nanotubes uniformly about 50 nm thick, and the loading of MnO_2 on the CNTs reaches 84%. Furthermore, the supercapacitive performances were investigated by cyclic voltammogram (CV), galvanostatic charge−discharge, and electrochemical impedance spectroscopy (EIS). The experimental results indicate that the composite exhibits not only high specific capacitance of 201 F g^{-1} and rate capability (the specific capacitance at 20 A g^{-1} is 70% of that at 1 A g^{-1}), but also excellent cycle stability (no obvious capacitance decay after 10 000 cycles at 1 A g^{-1}). An asymmetric electrochemical capacitor was assembled by using the obtained MnO_2/CNTs composite as positive electrode and activated carbon (AC) as negative electrode. The as-assembled AC//MnO_2/CNTs capacitor can cycle reversibly in a voltage of 0−1.5 V and give a high energy density of 13.3 Wh kg^{-1} at a power density of 600 W kg^{-1}.

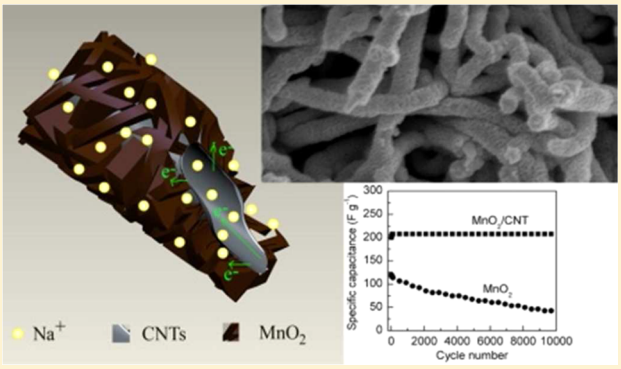

INTRODUCTION

Recently, climate change and the depletion of fossil fuels have compelled us to develop alternative energy storage/conversion devices with high power and energy densities.[1,2] Supercapacitors, as a kind of attractive energy storage/conversion device, filled the gap between batteries and conventional solid-state and electrolytic capacitors because of their high power density, fast charging/discharging rate, and excellent cycle stability.[3−6] According to the charge storage mechanisms, one kind of supercapacitors is called electrical double-layer capacitors (EDLCs), including various carbon materials, which stores energy via ion adsorption at the electrode/electrolyte interface. Among these carbon materials, graphene and CNTs are considered as potential electrode materials for supercapacitors due to their superior electrical conductivity, high electrochemical stability, good mechanical properties, high specific surface area, and so on. However, the electrode systems composed of only graphene or CNTs have low energy density and capacitance.[7−9] Another kind of supercapacitors is known as pseudocapacitors, including transition-metal oxides and conducting polymers, which uses fast and reversible surface or near-surface redox reactions for charge storage. Among various transition metal oxides, MnO_2 has attracted much attention because of its abundance, low cost, environmental friendliness, rich redox activity, and high theoretical specific capacitance (1232 F g^{-1}).[10−12] In addition, unlike RuO_2, NiO, and Co_3O_4, MnO_2 can not only function well in neutral aqueous electrolytes rather than strong acidic or alkaline electrolytes, but also show a fast charge−discharge capability, analogous to non-Faradaic energy storage behavior, which is based on surface adsorption of electrolyte cations M^+ (Na^+, K^+, et al.) as well as proton incorporation according to the reaction:[6,10,13]

$$MnO_2 + xM^+ + yH^+ + (x + y)e^- \leftrightarrow MnOOM_xH_y$$

Obviously, it is similar to the charge storage mechanism of hydrous RuO_2. So MnO_2 is considered as a promising substitute for RuO_2 in the application of supercapacitors. However, the practical applications of MnO_2 are limited because of its low specific capacitance and insufficient cycling stability, which can be attributed to its poor electrical conductivity and the cycling crystal expansion/contraction induced by flaking off during repeated cycling processes.[9,14]

To overcome these disadvantages, the conducting carbon materials (e.g., graphene, CNTs) were used as supporting materials to form composites with MnO_2. Researchers have

Received: June 10, 2014
Revised: September 10, 2014
Published: September 10, 2014

Downloaded via LANZHOU BRANCH NATL SCIENCE LBRY on December 1, 2020 at 01:19:27 (UTC).
See https://pubs.acs.org/sharingguidelines for options on how to legitimately share published articles.

© 2014 American Chemical Society

dx.doi.org/10.1021/jp505744p | J. Phys. Chem. C 2014, 118, 22865−22872

reported several meaningful results concerned with MnO_2-based composites. For example, Chou et al. electrodeposited MnO_2 nanowires on the CNT paper by a cyclic voltammetric technique and obtained the composite with specific capacitance of 107.9 F g^{-1}. The results also indicated that the loading amount of MnO_2 reached 19.8% and the electrode lost 12% of initial capacitance after 3000 cycles.[15] Jin et al. successfully made nanocrystalline MnO_2 grow both on the surface and in the cavity of CNTs and found that the CNT−65 wt % MnO_2 sample revealed the specific capacitance up to 144 F g^{-1}.[16] Wang et al. synthesized MnO_2/CNT composite by a facile direct redox reaction. The composite with 44.4% MnO_2 showed the specific capacitance of 119.3 F g^{-1} and kept 90% of its specific capacitance after 2000 cycles.[17] In the above-mentioned works, the specific capacitance was measured by the discharging curves under the galvanostatic model, and in the range from 108 to 144 F g^{-1}. There were also several investigations such as MWNT/MnO_2 nanocomposite ultrathin film via redox deposition of MnO_2 on layer-by-layer assembled MWNT films,[18] MnO_2-multiwalled carbon nanotube films by electrophoretic deposition method,[19] a manganese dioxide/carbon nanotube composite fabricated using an in situ coating method,[20] and symmetrical MnO_2−carbon nanotube textile nanostructures,[21] where the specific capacitance was calculated by the CV curves. In this case, the calculated specific capacitance depended significantly on potential scan rates and even reached the value of more than 300 F g^{-1} at low scan rate. It should be pointed out that the mass loading is an important parameter for MnO_2/CNTs composites. As MnO_2 has low electrical conductivity and ion diffusion constant, its content is in inverse proportion to performance in the application of supercapacitors, which is confirmed in the report where the specific capacitance of MnO_2 can be reached as high as 1230 F g^{-1} at MnO_2 content of about 5% in weight but about 200 F g^{-1} for MnO_2 content of 67%.[22] However, depositing a thin MnO_2 layer on the surface of CNTs can provide good electrochemical performance with high mass-loading of the MnO_2 phase.[23] Yet for all that, it is still challenging to synthesize highly homogeneous and highly loading MnO_2/CNTs nanocomposites with high capacitance and long cyclic life. Chen et al. gave us a good strategy to generate a porous and branched hybrid of MnO_2/CNT a few years ago.[24] They also discussed the formation mechanism of the hybrid in detail through the optimal reaction conditions but did not involve any electrochemical issues. Herein, we use modified Chen's one-pot synthesis to obtain MnO_2/CNTs composite with high upper-capacitive performance. We greatly increase the mass ratio of potassium permanganate to carbon nanotubes in the synthesis reaction to enhance the loading of MnO_2. In the as-prepared composite, the cross-linked MnO_2 flakes on the carbon nanotubes form an open porous nanostructure, which is favorable for the intercalation/deintercalation of electrolyte cations into electrochemically active species. As a result, we can obtain a promising MnO_2/CNTs electrode material with high capacitance, ultralong cycling stability (no obvious capacitance decay after 10 000 cycles for 43 days at 1 A g^{-1}), and high loading of MnO_2. In a way, the present work shows and interprets that the microstructure of the resultant MnO_2/CNTs composite plays an important role in enhancing its capacitive performances.

EXPERIMENTAL SECTION

Preparation of the Composite MnO_2/CNTs. The MnO_2/CNTs composite was synthesized by a modified one-pot synthesis as follows:[24] 100 mg of commercial multiwalled CNTs (MWCNTs, Shenzhen Bier Co., Ltd., Shenzhen, China) and a certain amount of $KMnO_4$ (2.5 g) (A.R., Tianjin Baishi Chemical Industry Co., Ltd., Tianjin, China) were ground together in an agate mortar. The mixed powder then was dispersed in 100 mL of water with stirring for 10 min. 0.5 mL of concentrated H_2SO_4 was added to the above mixture with an additional 30 min of stirring. After that, the mixed solution was heated in an oil bath at 80 °C with continuous magnetic stirring for 1 h. The precipitate was collected by filtrating and washed repeatedly with deionized water after the mixture was cooled to room temperature. The solid product then was dried in a vacuum at 60 °C for 12 h to obtain MnO_2/CNTs composite. In our experiment, the amount of $KMnO_4$ is much larger than the one in the literature,[24] and the stirring times are also adjusted accordingly. Besides, the CNTs did not go through an additional acid treatment. In this case, the high loading of MnO_2 was achieved. For comparison, the pure MnO_2 was prepared by a similar procedure with adding alcohol instead of CNTs.

Materials Characterization. The images of samples were observed by field-emission scanning electron microscopy (FESEM; JSM-6701F, Japan) and transmission electron microscopy (TEM; TECNAI G2 TF20, U.S.). Their phase states were analyzed by X-ray diffraction (XRD; D/Max-2400, Japan) with Cu K_α radiation (λ = 1.5418 Å) operating at 40 kV, 100 mA. The components were determined by a Raman spectrum (BRUKER RFS 100/S, Germany). Chemical state analysis was performed by X-ray photoelectron spectroscopy (XPS; PHI-5702, U.S.). An Al K_α X-ray source, operating at 250 W with a pass energy of 29.35 eV, was utilized. Contact angle measurement for surface wettability study was carried out by HARKE-SPCA$_{x3}$ equipment with CMOS camera. Thermogravimetric (TG) analysis was carried out using a PerkinElmer TG/DTA-6300 instrument in the temperature range of 20−800 °C. A heating rate of 10 °C min^{-1} in air with a flow rate of 20 mL min^{-1} was used.

Preparation of Working Electrode. The working electrodes were prepared by coating mixtures of the MnO_2/CNT composites, acetylene black (Jiaozuo City Hexing Chemical Industry Co., Ltd., Henan, China), conducting graphite (Qingdao Chemyang graphite Co., Ltd., Shandong, China), and polytetrafluoroethylene (PTFE; Guangzhou Songbai Chemical Industry Co., Ltd., Guangdong, China) binder (weight ratio of 75:10:10:5) on a slice of carbon current collector (1 mm thick). Working electrode with a geometric surface area of about 1 cm^2 contained about 2 mg of MnO_2/CNT composite. The as-prepared electrode was dried at room temperature for 24 h.

Electrochemical Tests. The cyclic voltammetry (CV), electrochemical impedance spectroscopy (EIS), and galvanostatic charge−discharge tests of a working electrode were performed in a three-electrode cell, in which platinum foil and a saturated calomel electrode (SCE) were used as counter electrode and reference electrode, respectively, in 1 M Na_2SO_4 electrolyte. To further test the electrochemical performance of the composite in two-electrode, the AC//MnO_2/CNTs asymmetric capacitor was assembled, where AC, MnO_2/CNTs, and glass fiber served as negative electrode, positive

dx.doi.org/10.1021/jp505744p | J. Phys. Chem. C 2014, 118, 22865−22872

electrode, and separator, respectively. All of the above electrochemical measurements were carried out by using a CHI860D electrochemical working station.

Related Formula. The specific capacitance (C, F g^{-1}) of a single electrode in the three-electrode configuration is respectively calculated from the charge/discharge curves and the CV curves by using the formula:[10,25]

$$C = \frac{i \cdot t}{\Delta V} \quad (1)$$

$$C = \frac{\int i \cdot dV}{2v \cdot \Delta V} \quad (2)$$

where i (A g^{-1}) is current density, t (s) is the discharge time, ΔV (V) is the applied potential window, and v (mV S^{-1}) is the potential scan rate.

The mass ratio (R) between the positive and the negative electrodes in the two-electrode configuration is expressed as follows:[26,27]

$$R = \frac{m_+}{m_-} = \frac{C_- \cdot \Delta V_-}{C_+ \cdot \Delta V_+} \quad (3)$$

where m_+ and m_- are the mass, C_+ and C_- are the specific capacitance, and ΔV_+ and ΔV_- are the potential window for the positive and negative electrodes, respectively.

The total capacitance (C, F), average specific capacitance (C_s, F g^{-1}), power density (P, kW kg^{-1}), and energy density (E, Wh kg^{-1}) of the cell in the two-electrode configuration are calculated from the galvanostatic charge−discharge curves by using the formula:[28,29]

$$C = \frac{I \cdot t}{\Delta V} \quad (4)$$

$$C_s = \frac{4 \cdot C}{M} \quad (5)$$

$$E = \frac{0.5C(\Delta V)^2}{3.6} \quad (6)$$

$$P = \frac{E}{t} \quad (7)$$

where I (A) is the discharge current, t (s) is the discharge time, ΔV (V) is the applied potential window, and M (g) is the total mass of the two electrodes.

RESULTS AND DISCUSSION

The fabrication process for MnO_2/CNTs is discussed below. First, the CNTs, under stronger acidic conditions, can be oxidized by excess $KMnO_4$, and then graphene sheets can be partly cleaved from the walls of the oxidized CNTs. Following the intercalation of SO_4^{2-} ions, the graphene sheets were exfoliated partly.[24] A further redox reaction then occurred, where $KMnO_4$ served as oxidant and the partly exfoliated graphene sheets served as sacrificial reductant. The reaction is as follows:

$$4KMnO_4 + 3C + 2H_2SO_4 \rightarrow 4MnO_2 + 3CO_2 + 2K_2SO_4 + 2H_2O$$

Of the products, MnO_2 grows on the nearest graphene sheets, which are provided by the CNTs themselves. When the formed MnO_2 covered the graphene sheets, as a barrier, it will prevent further access of the MnO_4^- ions to the carbon underneath and promote the reaction on another free carbon surface. This process may lead to complete and homogeneous coverage of the available CNTs surface.[16] With the increase of the reaction temperature, the newly formed MnO_2 nuclei continuously deposit on the preformed MnO_2 nanocrystallines so that the flaky morphology becomes thickening and entangling, and finally develop the cross-linked structure on the CNTs surface.

XRD patterns of the pristine CNTs, MnO_2, and MnO_2/CNTs composite are shown in Figure 1. It can be seen that the

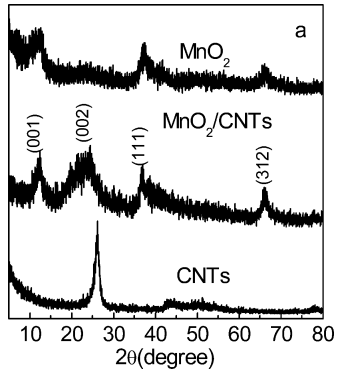

Figure 1. XRD patterns of the pristine CNTs, MnO_2, and MnO_2/CNTs composite.

pure CNTs show a sharp peak at around 26° and two broad weak peaks at around 44 and 52°, which are characteristic of graphite.[30] The four broad peaks of the MnO_2/CNTs at around 12, 24, 37, and 66° correspond to the crystal planes of (001), (002), (111), and (312) in birnessite-type MnO_2 (JCPDS 42-1317), respectively.[31] The characteristic peak of CNTs can be distinguished from the others on the XRD pattern of the MnO_2/CNTs, although its intensity is relatively weak. The two aspects are responsible for this. First, the weight percent of CNTs in the composite is only 16%; second, the diffraction peak of MnO_2 at around 24° is broadened and heightened, which overwhelms the signal of pure CNTs. A similar phenomenon is found in other reports.[17,32]

XPS was used to provide further evidence for the successful deposition of MnO_2 on CNTs surfaces and to examine the valent states of MnO_2 in MnO_2/CNTs composite (Supporting Information Figure S1). The manganese oxidation states are confirmed by analyzing the energy separation between the two peaks of Mn 3s doublet (ΔE), where Mn^{4+} and Mn^{3+} of MnO_2 were reported to have ΔE values of 4.78 and 5.41 eV, respectively.[21] As shown in Supporting Information Figure S1c, the ΔE of the as-deposited MnO_2 in MnO_2/CNTs composite is 4.96 eV, representing a coexistence of trivalence and tetravalence. It should be mentioned that some of the Mn^{4+} at the center of the MnO_6 octahedra are easy to replace by Mn^{3+} when a net negative charge is given. Meanwhile, the net negative charges compensated by the cations would lead to the formation of the birnessite phase.[33]

Raman analysis (Supporting Information Figure S2) confirms the existence of multiwalled carbon nanotubes with abundant structural defects in the composite.

The FESEM images of the pristine CNTs and MnO_2/CNTs composite are shown in Figure 2. From Figure 2a, it can be seen that the pristine CNTs exhibit regular morphology with a diameter of about 90−120 nm and the wall is smooth. Observed at low magnification of MnO_2/CNTs composite

dx.doi.org/10.1021/jp505744p | J. Phys. Chem. C 2014, 118, 22865−22872

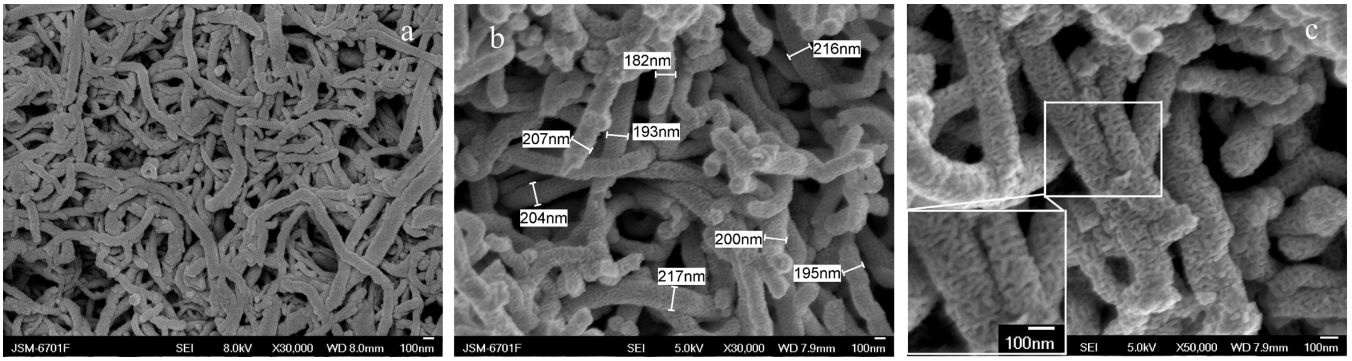

Figure 2. FESEM images of (a) the pristine CNTs, (b) low-magnification, and (c) high-magnification view of MnO_2/CNTs composite.

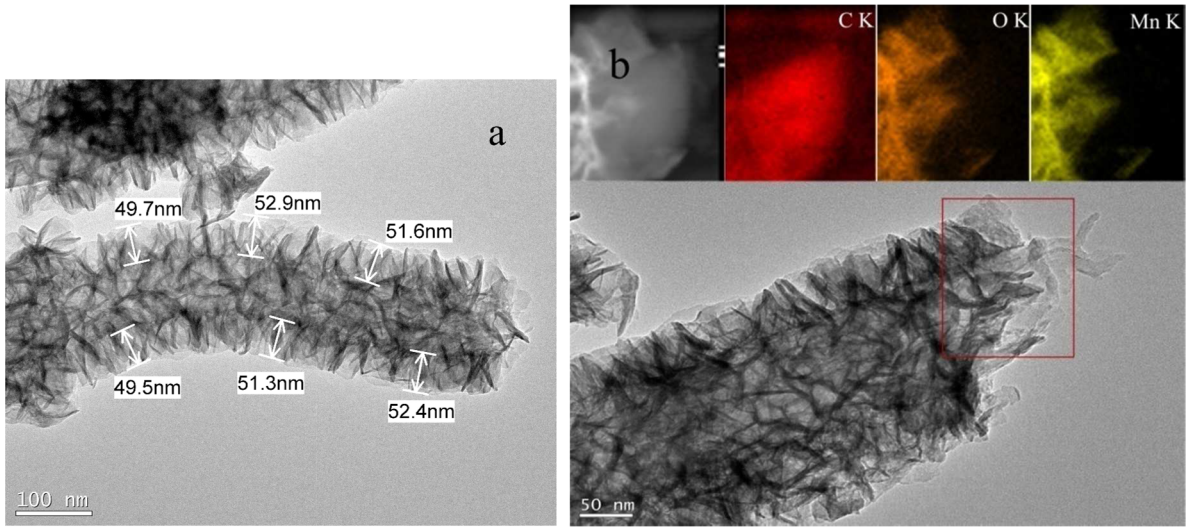

Figure 3. (a) TEM image and (b) elemental mapping data STEM image of MnO_2/CNTs composite.

(Figure 2b), we can found that the coated MnO_2 layer is uniform and the diameter of the nanotubes increases by about 100 nm as compared to the pristine CNTs, indicating that a MnO_2 layer 50 nm thick has been uniformly coated on the CNTs surface. Evaluated from the TGA measurement, the loading of MnO_2 on the CNTs is about 84% (Supporting Information Figure S3). At high magnification (Figure 2c), the cross-linked MnO_2 nanoflakes about 20 nm thick are clearly observed on the surface of CNTs, which provided abundant interstitial space in the composite. This unique structure can not only supply sufficient electrochemically active sites on the surface of MnO_2, but increase the effective liquid−solid interfacial area, provide a fast path for the insertion and extraction of electrolyte ions, and consequently facilitate the Faraday reaction. Meanwhile, the surface wettability of the composite has also improved. The measured water contact angle of the MnO_2/CNTs composite was about 46.3°, far less than that of the pure CNTs (114.2°) (Supporting Information Figure S4). It is well-known that the hydrophilic surface of the supercapacitor electrode material is an essential factor for better performance.[34]

To further analyze the morphology features of MnO_2/CNTs, we carry out TEM observation on the composite. As shown in Figure 3a, the cross-linked MnO_2 nanoflakes attached upon the sidewalls of the inner nanotubes uniformly, and the interfacial profiles between the nanoflakes and the tube can be well distinguished. The thickness of the MnO_2 layer is about 50 nm, which is in agreement with the FESEM results. It should be emphasized that, even after a long sonication time during preparation of the TEM specimen, the MnO_2 still attached on the CNTs surface, suggesting a strong interaction between MnO_2 and CNTs, which is due to the covalent bond and van der Waals interactions between them. The spatial distribution of Mn, O, and C elements in the composite is examined with elemental mapping analysis. As illustrated in Figure 3b, besides strong signal of the CNTs inner core, we can find that the C, O, and Mn elements distribute homogeneously throughout the cross-linked nanoflakes sheath, implying that the nanosheets are composed of MnO_2 and C.

The CVs of the MnO_2/CNTs, MnO_2, and CNTs in 1 M Na_2SO_4 electrolyte at 50 mV s^{-1} are shown in Figure 4a. It is clearly seen that the CV curve of the MnO_2 shows basically rectangular shapes because of the fast, reversible successive surface redox reactions of MnO_2 phase,[6] demonstrating typical pseudocapacitive behavior in neutral electrolyte, which is similar to the other reported results.[10,35] However, the CV curve of the MnO_2/CNTs exhibits rectangular shape with weak redox peaks similar to the earlier research.[11] We deduced that the intimate bonding of the cross-linked MnO_2 and CNTs minimizes the contact resistance between them so that Faraday processes of the electrochemically active species become easy. Furthermore, the coexistence of Mn^{3+} and Mn^{4+} states, as indicated in the XPS result, implies that not only the surface adsorption on the MnO_2 occurs but also the other redox

dx.doi.org/10.1021/jp505744p | J. Phys. Chem. C 2014, 118, 22865−22872

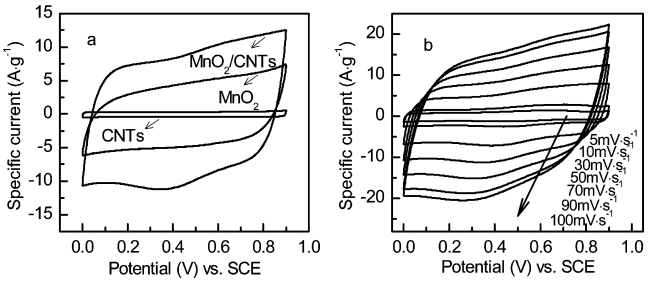

Figure 4. CV curves of (a) the MnO_2/CNTs, MnO_2, and CNTs at the scan rate of 50 mV s^{-1}, and (b) the MnO_2/CNTs at different scan rates.

reaction occurs due to the low valence state of Mn. It also can be observed that the CV loop of the MnO_2/CNTs is much larger than that of MnO_2 and CNTs. Generally, the integral area of CV curves at the same scanning rate is proportional to specific capacitance. Therefore, the composite is enhanced in the capacitance because the conductive CNTs and pseudocapacitive MnO_2 form a positive synergistic effect. Besides, the unique structure of MnO_2/CNT composite can provide fast transport and facile accessibility to active sites for electrolyte species.[36] As shown in Figure 4b, the distortion of CV curves is unconspicuous even at the high scanning rate, implying that the system of electrodes has low contact resistance.

Figure 5a shows galvanostatic discharge curves of the MnO_2/CNTs, MnO_2, and CNTs in the potential range from 0 to 0.9 V (vs SCE) at the specific current of 1 A g^{-1}. It is noted that all of the curves are nearly linear besides the MnO_2/CNTs with weak plateau, which corresponds well with the discussions in the CV curves. According to eq 1, we can calculate the capacitance values at different specific currents from discharging time. The results indicate that the MnO_2/CNTs achieve higher specific capacitance (201 F g^{-1}) at 1 A g^{-1} than CNTs (8.7 F g^{-1}) and MnO_2 (124.9 F g^{-1}). The BET results indicate that specific surface area (71 m^2 g^{-1}, Supporting Information Figure S5c) of the MnO_2/CNTs composite is larger than that of pristine CNTs (51 m^2 g^{-1}, Supporting Information Figure S5a) but much less than that of pure MnO_2 (317 m^2 g^{-1}, Supporting Information Figure S5b). However, the composite has double porous structure consisting of mesopores with mean pore size of 2.5 nm and open pores ranging from 10 to 30 nm (Supporting Information Figure S5d). The significantly enhanced capacitance is probably attributed to the synergistic effect between CNTs and MnO_2, and unique structure of the composite. First, the CNTs enable one to improve the overall conductivity of the composite because they can provide continuous charge transfer pathways. Second, the homogeneous and MnO_2 nanoflakes 20 nm thick are beneficial to elevate the usability of the active matters so that the electrochemical performance of the composite is improved. Third, the cross-linked MnO_2 nanoflakes can be in contact with CNTs through the partly exfoliated graphene, which is of good electrical conductivity and shortens the diffusion paths of the electron. Last, the three-dimensional porous network structure, formed through the interconnecting MnO_2 nanoflakes on the surface of CNTs, is able to effectively increase the liquid−solid interfacial reaction area or the electrochemically active sites, and provide a fast path for the Na^+ in the electrolyte to intercalate and deintercalate in the electroactive matters.

Figure 5b shows galvanostatic discharge curves of the MnO_2/CNTs at various specific currents. According to the discharging time, specific capacitances are estimated to be 201, 188, 179, 173, 164, 152, and 140 F g^{-1} at the current density of 1, 3, 5, 7, 10, 15, and 20 A g^{-1}, respectively. The specific capacitance of pristine CNTs, MnO_2, and MnO_2/CNTs composite as a function of specific current is shown in Figure 5c. It is clear that the specific capacitance for pure MnO_2 fades greatly with increasing specific current, indicating that poor rate capability is a feature of MnO_2 electrode materials with low electrical conductivity. The pristine CNTs show a low specific capacitance that is less sensitive to specific current. It is also seen for the MnO_2/CNTs that the retention of 70% is achieved under high specific capacitance when specific current increases from 1 to 20 A g^{-1}. This is very important for improving power density at high energy density in the application of supercapacitors.

Typical complex plane plots for MnO_2/CNTs, MnO_2, and CNTs are presented in Figure 6; the frequency ranged from 0.1

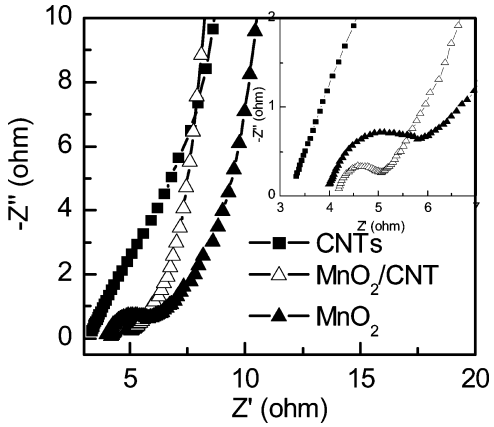

Figure 6. Nyquist plots of the MnO_2/CNTs, MnO_2, and CNTs.

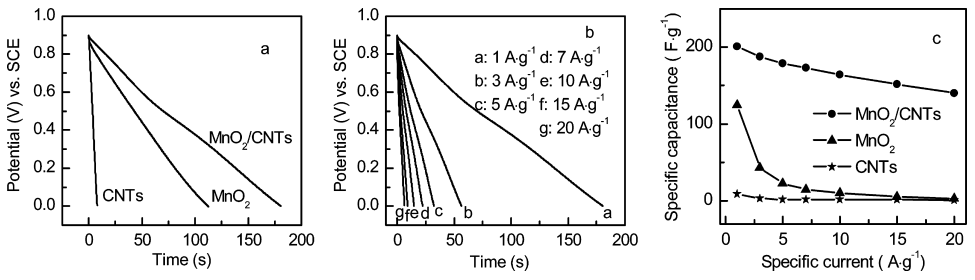

Figure 5. Galvanostatic discharge curves of (a) the MnO_2/CNTs, MnO_2, and CNTs at 1 A g^{-1}, (b) galvanostatic discharge curves, and (c) specific capacitance of the pristine CNTs, MnO_2, and MnO_2/CNTs at different specific currents.

dx.doi.org/10.1021/jp505744p | J. Phys. Chem. C 2014, 118, 22865−22872

Hz to 10 kHz at a bias of 0.4 V vs SCE reference electrode. We can find that complex plane plots for MnO_2/CNTs and MnO_2 show a very small semicircle in the high frequency region, implying light electrochemical polarization. Also, the diameter of the semicircle corresponds to the charge transfer resistance (R_{ct}) at the electrode/electrolyte interface.[37] As seen from the inset of Figure 6, the MnO_2/CNTs composite exhibited smaller R_{ct} than MnO_2. It may be attributed to the special structure of the MnO_2/CNTs composite, which facilitates the penetration of the electrolyte into the electrode and greatly increases the interface between the electrode and electrolyte. In the low-frequency region, the finite slope of the straight line represents the diffusive resistance of the electrolyte in the electrode pores.[37] It can be seen that the slope of the straight line for the MnO_2/CNTs composite is much bigger than that of the MnO_2 electrode, suggesting the MnO_2/CNTs electrode has lower diffusive resistance of the electrolyte and faster ion transport speed than the MnO_2 electrode.

Cycle life is an important parameter of supercapacitors. The excellent cycle stability of the MnO_2/CNTs was confirmed by the charging−discharging data. Figure 7 presents the variety of

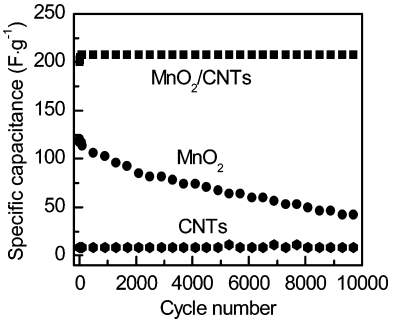

Figure 7. Cycle lifetime of the MnO_2/CNTs, MnO_2, and pure CNTs at 1 A g^{-1}.

specific capacitance with charging−discharging cycle numbers at 1 A g^{-1} in 1 M Na_2SO_4 aqueous solution. It can be found that both composite and pristine CNTs show much better cyclic stability than the pure MnO_2. However, the specific capacitance of the CNTs is far less than that of the composite. Obviously, the MnO_2/CNTs electrode reveals excellent performance in term of specific capacitance and cyclic life. During the first 100 cycles, the specific capacitance of the MnO_2/CNTs electrode slightly increases with cycling numbers, implying that the full relief of the composite's pseudocapacitance needs a so-called activated process. The intercalation/deintercalation of the electrolyte ions within the MnO_2/CNTs electrode will tend to be more complete by means of the initial charging/discharging process, so that active sites of the electrode materials increase and hence the specific capacitance is enhanced.[38,39] After the electrochemically active materials are activated, the specific capacitance is maintained at the same value over the next 9900 cycles. Thus, over 10 000 cycles for 43 days, the composite can maintain the capacitance without decaying. This contrasts with experimental results about other kinds of MnO_2/CNTs electrodes, where there is 5−20% degradation of the capacitance in 500−3000 cycle tests.[12,32,40] We postulate three effects on promoting a high capacitance and a long cycle life for the MnO_2/CNTs composites. First, the CNTs and the partly exfoliated graphene coming from them serve as conductive matrix and networks to promote fast Faradaic charging and discharging of the MnO_2 nanoflakes. Second, the porous nanostructure of the cross-linked MnO_2 layer on the surface of CNTs can effectively accommodate a large volume change during cycling to suppress the fast capacity fading. Third, the interconnected MnO_2 nanoflakes, tightly attached upon the CNTs matrix through those partly exfoliated graphene, reinforce the material structure to withstand the structure collapse upon cycling.

High-performance supercapacitors are expected to be operated with high voltage, high energy density, and long cycle life in the future.[41,42] An asymmetric supercapacitor is a promising design strategy with high voltage and high energy density.[14] Herein, an asymmetric supercapacitor device was assembled on the basis of AC as a negative electrode and MnO_2/CNTs as a positive electrode using 1 M Na_2SO_4 solution as electrolyte.

To evaluate the electrochemical properties and quantify the specific capacitance of the as-prepared AC//MnO_2/CNTs capacitor, we performed cyclic voltammogram (CV) measurements on these two-electrode materials using a three-electrode system (Figure 8a). As illustrated in the figure, the CV curve of

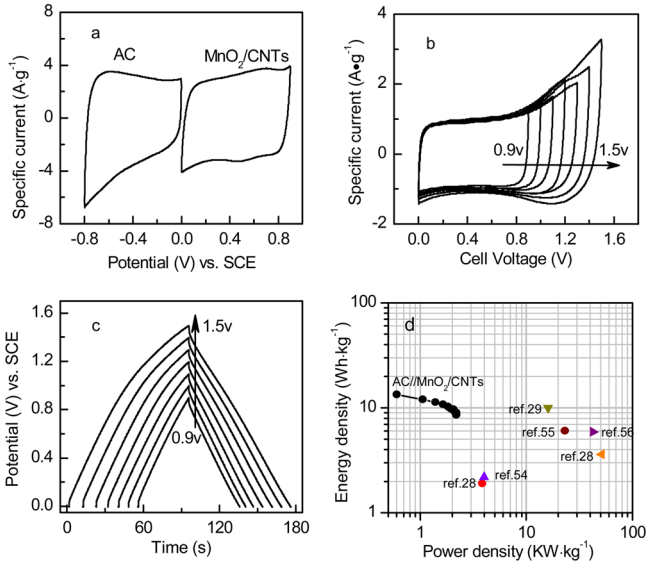

Figure 8. (a) Comparative cyclic voltammograms of AC and MnO_2/CNTs electrodes in a three-electrode system at a scan rate of 10 mV s^{-1}. (b) Cyclic voltammograms of the asymmetric supercapacitor of AC//MnO_2/CNTs measured at different potential windows at a scan rate of 10 mV s^{-1}. (c) Galvanostatic charge−discharge characteristics of asymmetric supercapacitor at a current density of 1 A g^{-1} in 1 mol L^{-1} Na_2SO_4. (d) Ragone plot of the asymmetric (AC//MnO_2/CNTs) capacitor as compared to data in other literature.

AC electrode in the potential window of −0.8 to 0 V exhibits a nearly rectangular shape without detectable redox peaks, indicating a typical characteristic of electric double layer (EDL). The CV shape of the MnO_2/CNTs electrode in the potential range of 0−0.9 V illustrates that the overall capacitance derives from the combined contribution of the pseudocapacitance of MnO_2 and the EDL capacitance of CNTs in the composite. Moreover, the CV curve of the MnO_2/CNTs electrode exhibits nearly a mirror-image current response on voltage reversal, indicating a good reversibility.[43] On the basis of the CVs (Figure 8a), the specific capacitance of the AC and MnO_2/CNT composite electrodes is estimated as 39 and 140 F g^{-1}, respectively. In addition, the lower-limit potential of AC

dx.doi.org/10.1021/jp505744p | J. Phys. Chem. C 2014, 118, 22865−22872

electrode and the upper-limit potential of MnO_2/CNTs electrode can basically reach −0.8 and 0.9 V, respectively, without obvious polarizations, and thus the theoretical maximum potential window of the AC//MnO_2/CNTs capacitor can reach 1.7 V. Here, the practical potential window could be increased to 1.5 V to achieve better electrochemical properties (Figure 8b). In an asymmetric capacitor, for getting an optimum cell voltage, a mass balance between the positive and negative electrodes will be necessary. According to eqs 2 and 3, the mass ratio of the composite to AC was selected to be 0.25 in the asymmetric capacitor. Figure 8c shows the typical charge−discharge curves of the asymmetric capacitor of AC//MnO_2/CNTs measured at 1 A g^{-1}. Clearly, the curves are close to an isosceles triangle due to the intrinsic reversibility of AC and MnO_2/CNTs in the testing electrolyte. Note that the cell voltage of this asymmetric supercapacitor can be up to 1.5 V.

It is well-known that the enlarged potential window is beneficial for enhancing energy density of the materials. Accordingly, the energy density of 13.3 Wh kg^{-1} and the power density of 600 W kg^{-1} are achieved using this asymmetric supercapacitor at operating voltages of 1.5 V, which were calculated by eqs 4−7. As compared to similar systems reported previously using symmetric AC//AC,[28,44] CNTs//CNTs,[45] MnO_2//MnO_2,[28] or other asymmetric AC//MnO_2,[29] polyaniline//MnO_2 supercapacitor,[46] this asymmetric supercapacitor exhibits high energy density (Figure 8d). These results indicate that the MnO_2/CNTs composite is a very promising electrode material for assembling asymmetric supercapacitors device with both high energy and high voltage.[35]

CONCLUSIONS

The MnO_2/CNTs composite is generated by modified chemical method in a mild one-pot reaction process. The cross-linked MnO_2 layer attaches upon the sidewalls of the inner nanotubes uniformly about 50 nm thick. The composite exhibits a higher specific capacitance (201 F g^{-1} at 1 A g^{-1}), higher rate capability (140 F g^{-1} at 20 A g^{-1}), and outstanding capacitance retention upon cycling (no decay after 10 000 cycles at 1 A g^{-1}) than that of pristine MnO_2 in a neutral electrolyte. The as-assembled AC//MnO_2/CNTs capacitor exhibits a wide working voltage (1.5 V), high power, and energy densities (600 W kg^{-1} and 13.3 Wh kg^{-1} at 1 A g^{-1}). Consequently, the MnO_2/CNTs composite is a very promising electrode material for assembling capacitor with both high energy and good capacitance retention.

ASSOCIATED CONTENT

Supporting Information

XPS spectra; Raman spectrum; TG data for composite; wettability test of composite and pure CNTs; nitrogen adsorption−desorption isotherms; and BJH pore size distributions plot of the pristine CNTs, pure MnO_2, and the composite. This material is available free of charge via the Internet at http://pubs.acs.org.

AUTHOR INFORMATION

Corresponding Author

*Tel.: +86 931 7973255. Fax: +86 931 8859764. E-mail: zhongai@nwnu.edu.cn.

Notes

The authors declare no competing financial interest.

ACKNOWLEDGMENTS

We gratefully acknowledge the financial support offered by the National Natural Science Foundation of China (nos. 20963009 and 21163017), Specialized Research Fund for the Doctoral Program of Higher Education (no. 20126203110001), Fundamental Research Funds for the Central Universities (no. zyz2012064), and the Natural Science Foundation of Gansu Province, China (no. 1308RJZA261).

REFERENCES

(1) Wang, H. W.; Hu, Z. A.; Chang, Y. Q.; Chen, Y. L.; Zhang, Z. Y.; Yang, Y. Y.; Wu, H. Y. Preparation of Reduced Graphene Oxide/Cobalt Oxide Composites and Their Enhanced Capacitive Behaviors by Homogeneous Incorporation of Reduced Graphene Oxide Sheets in Cobalt Oxide Matrix. *Mater. Chem. Phys.* **2011**, *130*, 672−679.

(2) Teng, F.; Santhanagopalan, S.; Meng, D. D. Microstructure Control of MnO_2/CNT Hybrids under In-situ Hydrothermal Conditions. *Solid State Sci.* **2010**, *12*, 1677−1682.

(3) Gao, H.; Xiao, F.; Ching, C. B.; Duan, H. High-Performance Asymmetric Supercapacitor Based on Graphene Hydrogel and Nanostructured MnO_2. *ACS Appl. Mater. Interfaces* **2012**, *4*, 2801−2810.

(4) Yang, Y.; Hu, Z.; Zhang, Z.; Zhang, F.; Zhang, Y.; Liang, P.; Zhang, H.; Wu, H. Reduced Graphene Oxide−nickel Oxide Composites with High Electrochemical Capacitive Performance. *Mater. Chem. Phys.* **2012**, *133*, 363−368.

(5) Bose, S.; Kuila, T.; Mishra, A. K.; Rajasekar, R.; Kim, N. H.; Lee, J. H. Carbon-based Nanostructured Materials and Their Composites as Supercapacitor Electrodes. *J. Mater. Chem.* **2012**, *22*, 767−784.

(6) Simon, P.; Gogotsi, Y. Materials for Electrochemical Capacitors. *Nat. Mater.* **2008**, *7*, 845−854.

(7) Dillon, A. C. Carbon Nanotubes for Photoconversion and Electrical Energy Storage. *Chem. Rev.* **2010**, *110*, 6856−6872.

(8) Teng, F.; Santhanagopalan, S.; Wang, Y.; Meng, D. D. In-situ Hydrothermal Synthesis of Three-dimensional MnO_2−CNT Nanocomposites and Their Electrochemical Properties. *J. Alloys Compd.* **2010**, *499*, 259−264.

(9) Yun, Y. S.; Kim, J. M.; Park, H. H.; Lee, J.; Huh, Y. S.; Jin, H. Free-standing Heterogeneous Hybrid Papers Based on Mesoporous γ-MnO_2 Particles and Carbon Nanotubes for Lithium-ion Battery Anodes. *J. Power Sources* **2013**, *244*, 747−751.

(10) Li, H. H.; Zhang, X. D.; Ding, R.; Qi, L.; Wang, H. Y. Facile Synthesis of Mesoporous MnO_2 Microspheres for High Performance AC//MnO_2 Aqueous Hybrid Supercapacitors. *Electrochim. Acta* **2013**, *108*, 497−505.

(11) Shimamoto, K.; Tadanaga, K.; Tatsumisago, M. All-solid-state Electrochemical Capacitors Using MnO_2/Carbon Nanotube Composite Electrode. *Electrochim. Acta* **2013**, *109*, 651−655.

(12) Wang, H. J.; Peng, C.; Zheng, J. D.; Peng, F.; Yu, H. Design, Synthesis and the Electrochemical Performance of MnO_2/C@CNT as Supercapacitor Material. *Mater. Res. Bull.* **2013**, *48*, 3389−3393.

(13) Wang, Y. H.; Liu, Y. S.; Zhitomirsky, I. Surface Modification of MnO_2 and Carbon Nanotubes Using Organic Dyes for Nanotechnology of Electrochemical Supercapacitors. *J. Mater. Chem. A* **2013**, *1*, 12519−12526.

(14) Jin, Y.; Chen, H. Y.; Chen, M. H.; Liu, N.; Li, Q. W. Graphene-Patched CNT/MnO_2 Nanocomposite Papers for The Electrode of High-Performance Flexible Asymmetric Supercapacitors. *ACS Appl. Mater. Interfaces* **2013**, *5*, 3408−3416.

(15) Chou, S. L.; Wang, J. Z.; Chew, S. Y.; Liu, H. K.; Dou, S. X. Electrodeposition of MnO_2 Nanowires on Carbon Nanotube Paper as Free-standing, Flexible Electrode for Supercapacitors. *Electrochem. Commun.* **2008**, *10*, 1724−1727.

(16) Jin, X. B.; Zhou, W. Z.; Zhang, S. W.; Chen, G. Z. Nanoscale Microelectrochemical Cells on Carbon Nanotubes. *Small* **2007**, *3*, 1513−1517.

(17) Wang, H.; Peng, C.; Peng, F.; Yu, H.; Yang, J. Facile Synthesis of MnO_2/CNT Nanocomposite and Its Electrochemical Performance for Supercapacitors. *Mater. Sci. Eng., B* **2011**, *176*, 1073−1078.
(18) Lee, S. W.; Kim, J.; Chen, S.; Hammond, P. T.; Yang, S. Carbon Nanotube/Manganese Oxide Ultrathin Film Electrodes for Electrochemical Capacitors. *ACS Nano* **2010**, *4*, 3889−3896.
(19) Su, Y.; Zhitomirsky, I. Electrophoretic Nanotechnology of Composite Electrodes for Electrochemical Supercapacitors. *J. Phys. Chem. B* **2013**, *117*, 1563−1570.
(20) Xie, X. F.; Gao, L. Characterization of A Manganese Dioxide/Carbon Nanotube Composite Fabricated Using an In Situ Coating Method. *Carbon* **2007**, *45*, 2365−2373.
(21) Hu, L. B.; Chen, W.; Xie, X.; Liu, N.; Yang, Y.; Wu, H.; Yao, Y.; Pasta, M.; Alshareef, H. N.; Cui, Y. Symmetrical MnO_2−Carbon Nanotube−Textile Nanostructures for Wearable Pseudocapacitors with High Mass Loading. *ACS Nano* **2011**, *5*, 8904−8913.
(22) Chen, W.; Rakhi, R. B.; Hu, L. B.; Xie, X.; Cui, Y.; Alshareef, H. N. High-Performance Nanostructured Supercapacitors on a Sponge. *Nano Lett.* **2011**, *11*, 5165−5172.
(23) Wei, W. F.; Cui, X. W.; Chen, W. X.; Ivey, D. G. Manganese Oxide-Based Materials as Electrochemical Supercapacitor Electrodes. *Chem. Soc. Rev.* **2011**, 1697−1721.
(24) Chen, Y.; Zhang, Y.; Geng, D.; Li, R.; Hong, H.; Chen, J.; Sun, X. One-pot Synthesis of MnO_2 Graphene Carbon Nanotube Hybrid by Chemical Method. *Carbon* **2011**, *49*, 4434−4442.
(25) Xu, J.; Wang, Q. F.; Wang, X. W.; Xiang, Q. Y.; Liang, B.; Chen, D.; Shen, G. Z. Flexible Asymmetric Supercapacitors Based upon Co_9S_8 Nanorod//Co_3O_4@ RuO_2 Nanosheet Arrays on Carbon Cloth. *ACS Nano* **2013**, *7*, 5453−5462.
(26) Yan, J.; Fan, Z.; Sun, W.; Ning, G.; Wei, T.; Zhang, Q.; Zhang, R.; Zhi, L.; Wei, F. Advanced Asymmetric Supercapacitors Based on Ni (OH) $_2$/Graphene and Porous Graphene Electrodes with High Energy Density. *Adv. Funct. Mater.* **2012**, *22*, 2632−2641.
(27) Demarconnay, L.; Raymundo-Pīnero, E.; Béguin, F. Adjustment of Electrodes Potential Window in an Asymmetric Carbon/MnO_2 Supercapacitor. *J. Power Sources* **2011**, *196*, 580−586.
(28) Khomenko, V.; Raymundo-Pinero, E.; Beguin, F. Optimisation of an Asymmetric Manganese Oxide/Activated Carbon Capacitor Working at 2V in Aqueous Medium. *J. Power Sources* **2006**, *153*, 183−190.
(29) Brousse, T.; Taberna, P.; Crosnier, O.; Dugas, R.; Guillemet, P.; Scudeller, Y.; Zhou, Y.; Favier, F.; Bélanger, D.; Simon, P. Long-term Cycling Behavior of Asymmetric Activated Carbon/MnO_2 Aqueous Electrochemical Supercapacitor. *J. Power Sources* **2007**, *173*, 633−641.
(30) Xia, H.; Wang, Y.; Lin, J.; Lu, L. Hydrothermal Synthesis of MnO_2/CNT Nanocomposite with a CNT Core/Porous MnO_2 Sheath Hierarchy Architecture for Supercapacitors. *Nanoscale Res. Lett.* **2012**, *7*, 1−10.
(31) Ma, S. B.; Ahn, K. Y.; Lee, E. S.; Oh, K. H.; Kim, K. B. Synthesis and Characterization of Manganese Dioxide Spontaneously Coated on Carbon Nanotubes. *Carbon* **2007**, *45*, 375−382.
(32) Yan, J.; Fan, Z.; Wei, T.; Cheng, J.; Shao, B.; Wang, K.; Song, L.; Zhang, M. Carbon Nanotube/MnO_2 Composites Synthesized by Microwave-assisted Method for Supercapacitors with High Power and Energy Densities. *J. Power Sources* **2009**, *194*, 1202−1207.
(33) Zhang, J.; Jiang, J.; Zhao, X. S. Synthesis and Capacitive Properties of Manganese Oxide Nanosheets Dispersed on Functionalized Graphene Sheets. *J. Phys. Chem. C* **2011**, *115*, 6448−6454.
(34) Dubal, D. P.; Dhawale, D. S.; Salunkhe, R. R.; Fulari, V. J.; Lokhande, C. D. Chemical Synthesis and Characterization of Mn_3O_4 Thin Films for Supercapacitor Application. *J. Alloys Compd.* **2010**, *497*, 166−170.
(35) Zhu, G.; Deng, L.; Wang, J.; Kang, L.; Liu, Z. Hydrothermal Preparation and the Capacitance of Hierarchical MnO_2 Nanoflower. *Colloids Surf., A* **2013**, *434*, 42−48.
(36) Choi, B. G.; Huh, Y. S.; Hong, W. H.; Kim, H. J.; Park, H. S. Electrochemical Assembly of MnO_2 on Ionic Liquid−Graphene Films into a Hierarchical Structure for High Rate Capability and Long Cycle Stability of Pseudocapacitors. *Nanoscale* **2012**, *4*, 5394−5400.
(37) Fan, Y.; Zhang, X.; Liu, Y.; Cai, Q.; Zhang, J. One-pot Hydrothermal Synthesis of Mn_3O_4/Graphene Nanocomposite for Supercapacitors. *Mater. Lett.* **2013**, *95*, 153−156.
(38) Dai, Y. M.; Tang, S. C.; Vongehr, S.; Meng, X. K. Silver Nanoparticle-Induced Growth of Nanowire-Covered Porous MnO_2 Spheres with Superior Supercapacitance. *ACS Sustainable Chem. Eng.* **2014**, *48*, 3389−3393.
(39) Lu, X. H.; Zheng, D. Z.; Zhai, T.; Liu, Z. Q.; Huang, Y. Y.; Xie, S. L.; Tong, Y. X. Facile Synthesis of Large-area Manganese Oxide Nanorod Arrays as a High-performance Electrochemical Supercapacitor. *Energy Environ. Sci.* **2011**, *4*, 2915−2921.
(40) Bordjiba, T.; Bélanger, D. Development of New Nanocomposite Based on Nanosized-Manganese Oxide and Carbon Nanotubes for High Performance Electrochemical Capacitors. *Electrochim. Acta* **2010**, *55*, 3428−3433.
(41) Choi, B. G.; Yang, M.; Hong, W. H.; Choi, J. W.; Huh, Y. S. 3D Macroporous Graphene Frameworks for Supercapacitors with High Energy and Power Densities. *ACS Nano* **2012**, *6*, 4020−4028.
(42) Chen, P.; Shen, G.; Shi, Y.; Chen, H.; Zhou, C. Preparation and Characterization of Flexible Asymmetric Supercapacitors Based on Transition-Metal-Oxide Nanowire/Single-Walled Carbon Nanotube Hybrid Thin-Film Electrodes. *ACS Nano* **2010**, *4*, 4403−4411.
(43) Wu, Z.; Ren, W.; Wang, D.; Li, F.; Liu, B.; Cheng, H. High-energy MnO_2 Nanowire/Graphene and Graphene Asymmetric Electrochemical Capacitors. *ACS Nano* **2010**, *4*, 5835−5842.
(44) Wang, D. W.; Li, F.; Liu, M.; Lu, G. Q.; Cheng, H. M. 3D Aperiodic Hierarchical Porous Graphitic Carbon Material for High-Rate Electrochemical Capacitive Energy Storage. *Angew. Chem.* **2008**, *120*, 379−382.
(45) Kaempgen, M.; Chan, C. K.; Ma, J.; Cui, Y.; Gruner, G. Printable Thin Film Supercapacitors Using Single-Walled Carbon Nanotubes. *Nano Lett.* **2009**, *9*, 1872−1876.
(46) Khomenko, V.; Raymundo-Pinero, E.; Frackowiak, E.; Beguin, F. High-Voltage Asymmetric Supercapacitors Operating in Aqueous Electrolyte. *Appl. Phys. A: Mater. Sci. Process.* **2006**, *82*, 567−573.